Quantitative Surface Potential Measurements by AC Electrostatic Force Microscopy

Thomas Hackl, Mathias Poik and Georg Schitter *Senior Member, IEEE,*
Automation and Control Institute (ACIN), TU Wien
Vienna, Austria
hackl@acin.tuwien.ac.at

***Abstract*—Electric charge distributions and the associated surface potentials at the nanoscale play a key role in many areas from material sciences to biology. The increasing field of sample analysis in liquid environments of biologically relevant ionic concentration demands for invasive-free measurements, hardly achievable with current techniques. This paper presents the development of a novel Atomic force Microscopy measurement mode, termed AC-EFM, enabling quantitative surface potential measurements at the nanoscale. It circumvents the use of a dc-bias, which leads to parasitic electrochemical effects in liquids in conventional methods, by the application of an amplitude modulated high frequency voltage. The surface potential is measured through the shift in cantilever resonance frequency, which itself is detected by a phase-locked loop. Measurements with externally applied sample potentials validate the derived model and experiments on a standard KPFM sample show improved spatial resolution, when compared to conventional methods. The capability of AC-EFM to quantitatively measure surface potentials at the nanoscale without the use of a dc-bias is demonstrated.**

***Index Terms*—atomic force microscopy, electrostatic force microscopy, surface potential**

I. Introduction

Since its first introduction in 1986, atomic force microscopy (AFM) [1] has been used as an analysis tool in a wide variety of scientific fields, ranging from material science applications [2] to more recent usage in biological cell analysis [3], [4]. Since then, many AFM modes has evolved, enabling the measurement and characterization of intrinsic sample properties such as mechanical [5], magnetic [6] or electrical features [7] at the nanoscale. In the case of measuring electric surface charges or the associated potential distribution, several different techniques have been developed, among which kelvin probe force microscopy (KPFM) [8] is the most widely used.

In KPFM a conducting AFM cantilever is held in close proximity (few tens of nm) to a sample surface whose surface potential distribution is to be measured. The electrostatic force interaction on the cantilever is modulated by an ac-voltage, usually oscillating with the resonance frequency of the cantilever to maximize the signal-to-noise ratio (SNR) [9]. The cantilever deflection, resulting from this electrostatic force, is measured and controlled to zero by an additional dc-bias. This, in addition with a lateral scan above the sample surface, results in a map of the samples potential distribution. However, due to this dc-bias, KPFM can not be used in aqueous media [10], which is important for e.g. biological AFM applications. A dc-electric field between cantilever and sample induces parasitic electrochemical effects, ranging from motion of the solvated ions to gas formation due to electrolysis [11] potentially damaging the sample and making any controlled measurement impossible.

Several derivations of KPFM have been developed in the recent years tackling this issue. Some of them circumvent the need for a dc-bias by completely omitting its use and by measuring the potential distribution in an open-loop configuration [12]. Another approach replaces the dc-bias with a second high frequency ac-voltage and uses its amplitude for the nullification of the electrostatic force [13], [14]. While these methods are generally able to operate in aqueous media [15], [16], they are still restricted to measurements in low-ionic concentrations ($\sim$10 mM). Higher concentrations of biological relevance ($>$100 mM) require excitation frequencies of several MHz [17], which is not achievable with the current limitation in cantilever design (i.e. resonance frequency). Only in this case a static and homogeneous medium between cantilever and sample is guaranteed, as induced motion of solvated ions in the liquid is suppressed.

A technically different but KPFM-related AFM measurement mode is electrostatic force microscopy (EFM) [18]. Here, no external electric signals are applied to the cantilever, which is solely mechanically excited and therefore enables its use in any medium. The electrostatic interaction with the sample potential manifests itself in a shift of the cantilever resonance frequency which is tracked and measured by means of a phase-locked loop (PLL). However, since no nullification of the electrostatic force is done, EFM only provides a qualitative measure of the potential distribution.

The contribution of this paper is the development of electrostatic force microscopy towards quantitative potential measurements. It adapts the use of the electrical cantilever excitation from KPFM, by employing an amplitude modulated high frequency ac-voltage. Its frequency is decoupled from the cantilever resonance frequency and can therefore be chosen arbitrarily-high. This eventually opens the possibility for invasive-free electric potential measurements in aqueous media of high ionic concentration. Here we present the basic principle and experimental setup of the developed mode, which

The financial support by the Austrian Science Fund FWF (Project Nr. P 31238-N28) and the FFG Production of the Future programme (Project Nr. 883916) of the Austrian BMK is gratefully acknowledged.

Pre-Print version of the article: T. Hackl, M. Poik and G. Schitter, "Quantitative Surface Potential Measurements by AC Electrostatic Force Microscopy,", 2023. DOI: 10.1109/I2MTC53148.2023.10176066

is termed AC-EFM. Its capability of quantitative potential measurements is verified and nanoscale spatial resolution is demonstrated by measurements on suitable metal structures in air.

II. Principle of AC-EFM

The electrostatic force F, arising from a potential difference of the sample and the cantilever, with its gradient $\partial F/\partial z$, changes the fundamental resonance frequency $f_0 = 1/2\pi \cdot \sqrt{k/m^*}$ of a cantilever with a stiffness k and an effective mass m^* as follows [9]:

$$f_0' = \frac{1}{2\pi}\sqrt{\frac{k - \frac{\partial F}{\partial z}}{m^*}}. \tag{1}$$

For small force gradients $\partial F/\partial z \ll 1$, the square root can be taylor series expanded [19], resulting in a connection between the electrostatic force gradient and the resonance frequency shift Δf:

$$f_0' \approx f_0\left(1 - \frac{1}{2k}\frac{\partial F}{\partial z}\right) \rightarrow \Delta f = f_0 - f_0' = \frac{f_0}{2k}\frac{\partial F}{\partial z}. \tag{2}$$

Inserting the general expression of the electrostatic force $F = -1/2 \cdot \partial C/\partial z \cdot (\phi - U_C)^2$ into (2) results in following connection between the cantilever voltage U_C to the change in resonance frequency:

$$\Delta f = -\frac{f_0}{4k}\frac{\partial^2 C}{\partial z^2}(\phi - U_C)^2, \tag{3}$$

where C is the tip-sample capacitance at the separation z and ϕ the surface potential to be measured. As discussed in the introduction, with AC-EFM an amplitude modulated high frequency ac-voltage is applied to the cantilever:

$$U_C = a \cdot sin(\omega_L t) \cdot sin(\omega_H t), \tag{4}$$

where ω_L and ω_H denote the low frequency (Hz to kHz) amplitude modulation and the high frequency (MHz) drive signal, respectively. Inserting (4) into (3) results in several Δf components. The terms around ω_H are filtered by the limited bandwidth of the phase-locked loop (which is in the order of kHz), resulting in an observed resonance frequency shift of: $\Delta f = \Delta f_0 + \Delta \hat{f}_{2\omega_L} \cdot cos(2\omega_L t)$, where

$$\begin{aligned} \Delta f_0 &= -\frac{f_0}{4k}\frac{\partial^2 C}{\partial z^2}\left(\phi^2 + \frac{a^2}{4}\right), \\ \Delta \hat{f}_{2\omega_L} &= \frac{f_0}{4k}\frac{\partial^2 C}{\partial z^2}\frac{a^2}{4}. \end{aligned} \tag{5}$$

By simultaneously recording the static and dynamic frequency shift components (Δf_0 and $\Delta \hat{f}_{2\omega_L}$ respectively), the surface potential ϕ can be calculated using Eq. (6):

$$\phi = \pm\sqrt{\left(-\frac{\Delta f_0}{\Delta \hat{f}_{2\omega_L}} - 1\right) \cdot \frac{a^2}{4}}. \tag{6}$$

The process on how the individual components are extracted out of the Δf signal is explained in more detail in Section IV-B.

Like in conventional EFM, with this implementation the sign of the surface potential is lost due to the quadratic term ϕ^2 in Eq. (5). However, since in EFM or KPFM one is only interested in the relative change of ϕ throughout a measurement series, this issue can be mitigated when preventing zero-crossings of the surface potential. This can be achieved, e.g. by the choice of a suitable cantilever with a specific metal coating (i.e. work function), which adds an offset to the measurement.

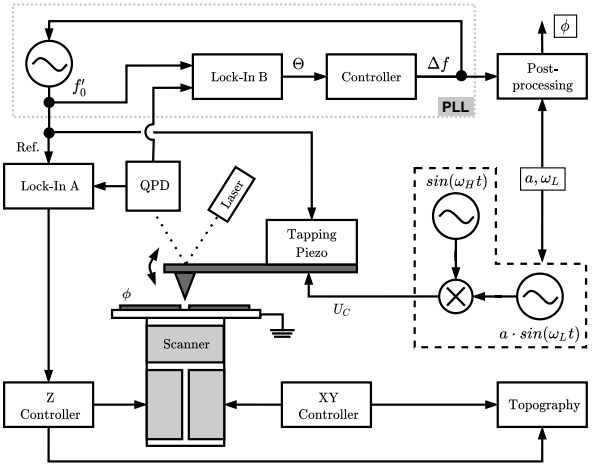

Fig. 1: Experimental setup of AC-EFM with the added components on the right side. A signal generator (dashed box) is used to generate U_C, which is applied to the mechanically oscillating cantilever. This voltage, together with the local surface potential ϕ, generates a force on the cantilever, detuning its phase response. The drive frequency, necessary to keep the phase of the cantilever oscillation constant (controlled by a PLL) is used in a post-processing step to calculate ϕ as described in the text.

III. Experimental Details

Figure 1 shows the schematic setup and control structure of the implemented AC-EFM technique. The measurement mode is implemented on a Multimode 8 AFM (Bruker, Santa Barbara, USA) with a Nanoscope V controller and a signal access module (SAM). It is operated in a two-pass process, where in the first pass the topography of a scan line is measured using intermittent-contact mode. In the second pass the same line is retraced at a certain tip-sample distance using the topography information gained in the first pass. During this second pass, the cantilever is mechanically excited at its resonance frequency f_0. Simultaneously, the AC-EFM signal U_C is applied to the conducting cantilever using an external signal generator (33522B, Keysight Technologies, USA). While scanning above the sample surface, the cantilever deflection phase Θ at the excitation frequency f_0' is held constant via a PLL as indicated in Fig. 1. The control signal Δf is recorded and used alongside the AC-EFM signal components (a, ω_L) and the scanning trajectory in a post-processing step

Pre-Print version of the article: T. Hackl, M. Poik and G. Schitter, "Quantitative Surface Potential Measurements by AC Electrostatic Force Microscopy,", 2023. DOI: 10.1109/I2MTC53148.2023.10176066

to calculate the surface potential distribution ϕ.
Overall gold coated cantilevers (TAP300GB-G, BudgetSensors, Bulgaria) with a measured resonance frequency in air of f_0 = 225.6 kHz and a stiffness of k = 22.88 Nm are used. If not otherwise stated, lift heights of 50 nm, drive amplitudes of a = 2 V and drive frequencies of $\omega_L = 2\pi \cdot 120$ Hz, $\omega_H = 2\pi \cdot 1$ MHz are used. Here, we want to emphasize that the choice of ω_H is not limited by the system and can be chosen to be much higher.
Measurements are performed on a standard KPFM sample (BudgetSensors, Bulgaria). This sample features stripes with alternating material (Aluminium and Gold) and equal height, separated by a 500 nm wide trench. This enables measurements of the materials work functions, while minimizing potential crosstalk of topographical features. In addition, it allows the application of external voltages, which is used to mimic known surface potential distributions.

IV. Results and Discussion

A. Model Verification

To verify the derived model as given by Eq. (3)-(6), parameter sweeps are performed and the resulting static and dynamic frequency shifts, Δf_0 and $\Delta \hat{f}_{2\omega_L}$, are recorded. Fig. 2(a) and (b) show the influence of the surface potential ϕ and the drive amplitude a on the static frequency shift Δf_0. The parabolic dependence is clearly visible, and fully overlaps with the theoretical fits. In Fig. 2(c) the amplitude of the dynamic frequency shift $\Delta \hat{f}_{2\omega_L}$ is shown as a function of the drive amplitude a. Again, as given by Eq. (5), it fits the theoretical formulation with no dependence on the surface potential ϕ.
These two measured components ($\Delta f_0, \Delta \hat{f}_{2\omega_L}$), together with the knowledge of the cantilever voltage U_C, are then used in the upcoming steps to calculate the quantitative surface potential ϕ as derived in Eq. (6).

B. Measurement Procedure

To be able to calculate the surface potential, the static and dynamic frequency shift components need to be extracted out of the recorded Δf signal. This process is visualized in Fig. 3. Here, the scanning motion of the AFM is disabled and an external rectangular voltage is applied to the sample, in order to mimic a surface potential distribution. In (a) the recorded Δf-Map is shown, where the amplitude of the applied signal is set as indicated. The cross-section of the applied voltage and measured frequency shift is shown in (b) and (c), respectively. Since the dynamic part of the frequency shift does not depend on ϕ, its amplitude stays constant throughout the measurement. The static frequency shift Δf_0 however, changes with the high and low side of the applied potential, as expected. The individual components of the signal are extracted by calculating the mean value and the spectral components over a predefined time-window. The length of this window defines the trade-off between measurement accuracy and speed and is chosen to be exactly one period of the dynamic frequency shift $\Delta f_{2\omega_L}$ (i.e. $^{2\pi}/_{2\omega_L}$).
The two components of each high- and low-section are extracted and given in Table I. From these values and the known drive amplitude a = 2 V, the potentials (ϕ_1, ϕ_2) are calculated, leading to the measured amplitude of the applied rectangular signal: $\Delta\phi = \phi_1 - \phi_2$. Good agreement between the applied signal amplitude and the measurement is observed, validating the ability of AC-EFM to quantitatively measure the samples surface potential.

C. Voltage accuracy and spatial resolution

With the working measurement procedure, accuracy and spatial resolution of AC-EFM are analyzed. Figure 4 shows the measured surface potential, again with the scanning motion

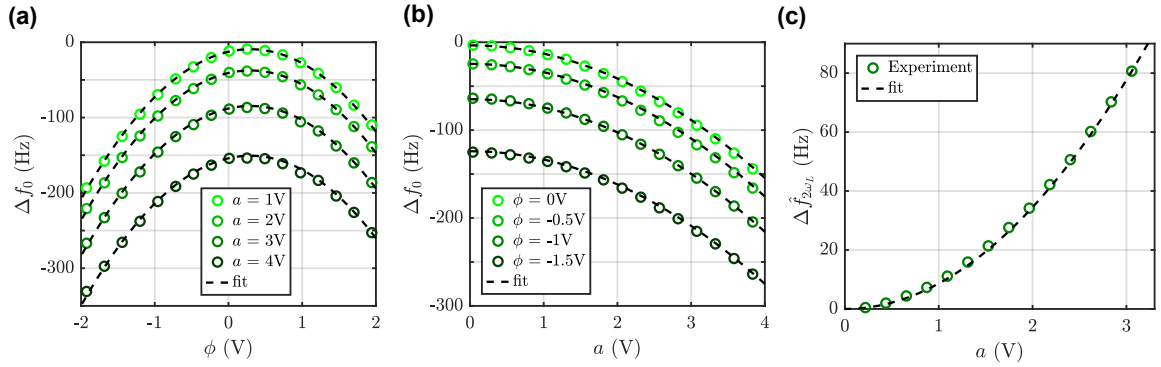

Fig. 2: **(a)** Dependence of the static frequency shift Δf_0 on the surface potential ϕ for different drive amplitudes a. **(b)** Dependence of the static frequency shift Δf_0 on the drive amplitude a for different surface potentials ϕ. **(c)** Dependence of the dynamic frequency shift $\Delta \hat{f}_{2\omega_L}$ on the drive amplitude a (surface potential ϕ has no impact). Dashed lines in each Figure represent fitted curves using Eq. (5) with f_0 = 225.6 kHz, k = 22.88 Nm and $\partial^2 C/\partial z^2$ = 0.0153. The offset of the parabolas in (a) to the zero point (0.28 V) can be explained by the natural work function difference between the varying materials of the cantilever and the sample.

Pre-Print version of the article: T. Hackl, M. Poik and G. Schitter, "Quantitative Surface Potential Measurements by AC Electrostatic Force Microscopy,", 2023. DOI: 10.1109/I2MTC53148.2023.10176066

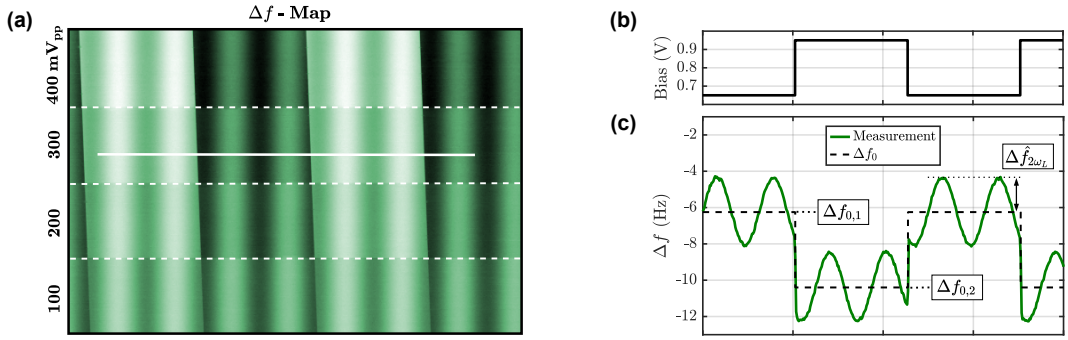

Fig. 3: **(a)** Measured Δf signal on a bare gold substrate with the xy-scanning motion disabled. Each vertical quarter represents a different amplitude of the applied voltage signal (given on the left), which is roughly synchronized with the line scanning rate. **(b)** Applied bias voltage at the cross section as indicated in (a), with the simultaneously measured Δf signal in **(c)**. The components Δf_0 and $\Delta \hat{f}_{2\omega_L}$ are highlighted for clarity. (extracted data in Table I)

Sample Bias (mVpp) + offset (V)	$\Delta f_{0,1}$ (Hz)	$\Delta f_{0,2}$ (Hz)	$\Delta \hat{f}_{2\omega_L}$ (Hz)	$\Delta\phi$ (mV)
400 + 0.8	-6.10	-11.66	1.86	**391**
300 + 0.8	-6.13	-10.29	1.86	**308**
200 + 0.8	-6.80	-9.61	1.86	**205**
100 + 0.8	-7.09	-8.45	1.86	**104**

TABLE I: Extracted data from Figure 3. The corresponding potentials ϕ are calculated for each section and their difference $\Delta\phi = \phi_1 - \phi_2$ is shown. Only minor deviations in the single mV range to the applied signal amplitude (highlighted) are observed.

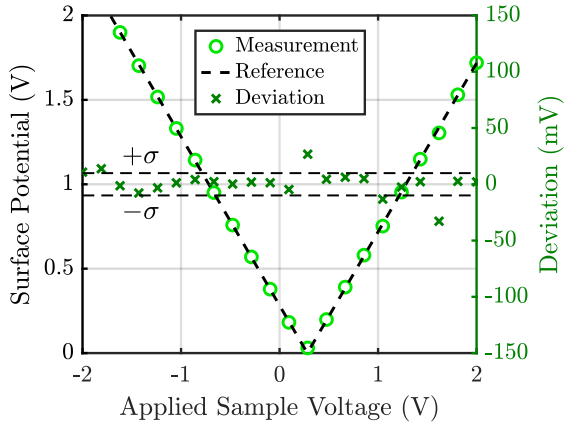

Fig. 4: Measured surface potential on a bare gold substrate using AC-EFM (only positive values shown) as a function of the applied sample voltage. The difference from the applied voltage is given on the right y-axis with a standard deviation of σ = 9.9 mV.

disabled, while linearly sweeping the applied voltage on the sample. As stated in the derivation of AC-EFM the sign of ϕ is lost during the measurement, explaining the two mirrored branches (only positive value shown) around the zero position at 0.28 V, which is again attributed to the natural difference in work function of the cantilever and sample metal coating. The difference of the measured surface potential to the known reference (i.e. the measurement error) is shown on the right y-axis and has a standard deviation over this 4 V range of σ = 9.9 mV, which is comparable to conventional KPFM measurements [20].

Assessing the spatial resolution of AC-EFM is done via measuring the work function distribution of a 5 µm wide aluminum stripe between two gold electrodes. Figure 5(a) shows the topography of the sample with the measured potential distributions using conventional KPFM and AC-EFM in (b) and (c), respectively. The most obvious difference between the two images is the increase in spatial resolution in AC-EFM. This arises from its dependence on the second derivative of the tip-sample capacitance (cf. Eq (3)) as opposed to the proportionality to its first derivative in standard KPFM. This effect is also exploited within frequency-modulated and heterodyne KPFM, which is discussed in more detail elsewhere [20]. In (c), the decreasing potential of the center-electrode (aluminum) towards its edges is attributed to be a result of non-uniform oxidation, which is generally more present at metal edges. Since gold is not subject to oxidation, this effect is not visible on the left and right electrode. Conventional KPFM in (b) on the other hand is not able to resolve this sample feature.

In summary it has been shown, that the introduced AFM mode enables a quantitative measurement of surface potential distributions at the nanoscale with the use of an amplitude modulated ac-voltage of arbitrarily choose-able carrier frequency. This development paves the way for electrical AFM measurements in aqueous solutions with biologically relevant ionic concentrations, which is part of ongoing and future work.

Pre-Print version of the article: T. Hackl, M. Poik and G. Schitter, "Quantitative Surface Potential Measurements by AC Electrostatic Force Microscopy,", 2023. DOI: 10.1109/I2MTC53148.2023.10176066

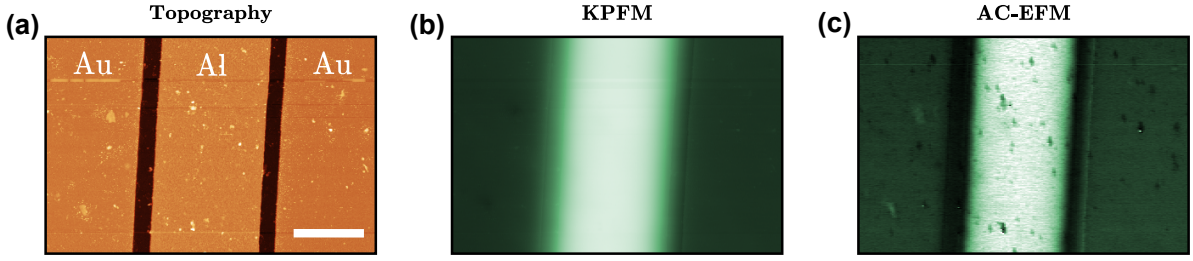

Fig. 5: **(a)** Measured Topography of the Gold-Aluminum sample. Some dust particles are visible on the sample surface (scale bar: 3 µm / color scale: 100 nm). **(b)** Measured potential distribution using conventional KPFM (color scale: 1.3 V). **(c)** Measured potential distribution using AC-EFM (color scale: 1.3 V).

V. Conclusion

The herein developed AFM measurement mode enables quantitative determination of distributed surface potentials on the nanoscale. An amplitude modulated high frequency signal is applied onto a mechanically oscillating AFM cantilever. This voltage, in combination with the sample potential, generates an electrostatic force that modifies the effective stiffness of the cantilever. The resulting change in resonance frequency is measured by a phase-locked loop and used in a post-processing step to calculate the surface potential distribution. Measurements on an aluminum-gold test sample validate the derived model and show measurement uncertainties of 9.9 mV.

With its use of a voltage whose carrier frequency can be arbitrarily chosen, AC-EFM is a promising candidate for surface potential measurements in aqueous solution of high ionic concentration, which is currently not possible with state of the art techniques. Future work will therefore focus on the adoption of the current setup for operation in liquid environment.

References

[1] G. Binnig, C. F. Quate, and C. Gerber, "Atomic force microscope," *Phys. Rev. Lett.*, vol. 56, pp. 930–933, Mar 1986.

[2] C. Örnek, C. Leygraf, and J. Pan, "Real-time corrosion monitoring of aluminum alloy using scanning kelvin probe force microscopy," *Journal of the Electrochemical Society*, vol. 167, no. 8, p. 081502, 2020.

[3] G. R. Heath, E. Kots, J. L. Robertson, S. Lansky, G. Khelashvili, H. Weinstein, and S. Scheuring, "Localization atomic force microscopy," *Nature*, vol. 594, no. 7863, pp. 385–390, Jun 2021.

[4] A. K. Sinensky and A. M. Belcher, "Label-free and high-resolution protein/dna nanoarray analysis using kelvin probe force microscopy," *Nature nanotechnology*, vol. 2, no. 10, pp. 653–659, 2007.

[5] M. P. Wenger, L. Bozec, M. A. Horton, and P. Mesquida, "Mechanical properties of collagen fibrils," *Biophysical Journal*, vol. 93, no. 4, pp. 1255–1263, 2007.

[6] M. Koblischka and U. Hartmann, "Recent advances in magnetic force microscopy," *Ultramicroscopy*, vol. 97, no. 1, pp. 103–112, 2003, proceedings of the Fourth International Conference on Scanning Probe Microscopy, Sensors and Nanostructures.

[7] A. Axt, I. M. Hermes, V. W. Bergmann, N. Tausendpfund, and S. A. L. Weber, "Know your full potential: Quantitative kelvin probe force microscopy on nanoscale electrical devices," *Beilstein journal of nanotechnology*, vol. 9, pp. 1809–1819, 2018.

[8] M. Nonnenmacher, M. P. O'Boyle, and H. K. Wickramasinghe, "Kelvin probe force microscopy," *Applied Physics Letters*, vol. 58, no. 25, pp. 2921–2923, 1991.

[9] U. Zerweck, C. Loppacher, T. Otto, S. Grafström, and L. M. Eng, "Accuracy and resolution limits of kelvin probe force microscopy," *Physical Review B*, vol. 71, no. 12, 2005.

[10] E. Strelcov, C. Arble, H. Guo, B. D. Hoskins, A. Yulaev, I. V. Vlassiouk, N. B. Zhitenev, A. Tselev, and A. Kolmakov, "Nanoscale mapping of the double layer potential at the graphene–electrolyte interface," *Nano Letters*, vol. 20, no. 2, pp. 1336–1344, Feb 2020.

[11] L. Collins, S. Jesse, J. I. Kilpatrick, A. Tselev, M. B. Okatan, S. V. Kalinin, and B. J. Rodriguez, "Kelvin probe force microscopy in liquid using electrochemical force microscopy," *Beilstein journal of nanotechnology*, vol. 6, pp. 201–214, 2015.

[12] N. Kobayashi, H. Asakawa, and T. Fukuma, "Quantitative potential measurements of nanoparticles with different surface charges in liquid by open-loop electric potential microscopy," *Journal of Applied Physics*, vol. 110, no. 4, p. 044315, 2011.

[13] D. Kohl, P. Mesquida, and G. Schitter, "Quantitative ac - kelvin probe force microscopy," *Microelectronic Engineering*, vol. 176, pp. 28–32, 2017.

[14] T. Hackl, G. Schitter, and P. Mesquida, "Ac kelvin probe force microscopy enables charge mapping in water," *ACS Nano*, vol. 16, no. 11, pp. 17 982–17 990, 2022.

[15] K. Honbo, S. Ogata, T. Kitagawa, T. Okamoto, N. Kobayashi, I. Sugimoto, S. Shima, A. Fukunaga, C. Takatoh, and T. Fukuma, "Visualizing nanoscale distribution of corrosion cells by open-loop electric potential microscopy," *ACS nano*, vol. 10, no. 2, pp. 2575–2583, 2016.

[16] T. Hackl, M. Poik, and G. Schitter, "Influence of imaging parameters on afm surface potential measurements in aqueous solutions," in *2022 IEEE 22nd International Conference on Nanotechnology (NANO)*, 2022, pp. 39–42.

[17] L. Collins, S. Jesse, J. I. Kilpatrick, A. Tselev, O. Varenyk, M. B. Okatan, S. A. L. Weber, A. Kumar, N. Balke, S. V. Kalinin, and B. J. Rodriguez, "Probing charge screening dynamics and electrochemical processes at the solid-liquid interface with electrochemical force microscopy," *Nature communications*, vol. 5, p. 3871, 2014.

[18] C. H. Lei, A. Das, M. Elliott, and J. E. Macdonald, "Quantitative electrostatic force microscopy-phase measurements," *Nanotechnology*, vol. 15, no. 5, p. 627, mar 2004.

[19] T. Glatzel, S. Sadewasser, and M. Lux-Steiner, "Amplitude or frequency modulation-detection in kelvin probe force microscopy," *Applied Surface Science*, vol. 210, no. 1-2, pp. 84–89, 2003.

[20] T. Hackl, M. Poik, and G. Schitter, "Heterodyne ac kelvin probe force microscopy for nanoscale surface potential imaging in liquids," *IEEE Transactions on Instrumentation and Measurement*, vol. 72, pp. 1–8, 2023.

Pre-Print version of the article: T. Hackl, M. Poik and G. Schitter, "Quantitative Surface Potential Measurements by AC Electrostatic Force Microscopy,", 2023. DOI: 10.1109/I2MTC53148.2023.10176066